

Ab Initio Studies of Structural and Vibrational Properties of Protonated Water Cluster H_7O_3^+ and Its Deuterium Isotopologues: An Application of Driven Molecular Dynamics

Martina Kaledin* and Christopher A. Wood

Chemistry and Biochemistry, Kennesaw State University, 1000 Chastain Road,
Box 1203, Kennesaw, Georgia 30144

Received March 3, 2010

Abstract: In this work, we present infrared (IR) spectra of H_7O_3^+ and its deuterium isotopomers calculated by direct molecular dynamics (MD) simulations at the B3LYP/6-31+G** computational level. The calculated spectra obtained at 100, 300, and 500 K were compared to available experimental observations, and spectral features were assigned using normal-mode analysis (NMA) and driven molecular dynamics (DMD). Spectral peaks at 2410 and 2540 cm^{-1} were assigned to asymmetric and symmetric stretches of the bridging hydrogen (BH) using NMA. The weak spectral features at 2166 and 2275 cm^{-1} were assigned to a combination band of BH asymmetric stretch, H_2O in phase wagging, OO stretch, and H_3O^+ rocking vibrations by DMD simulations. Our observation of BH stretch vibrations as low as 2166 cm^{-1} is in good agreement with the assignment of the low-resolution spectrum obtained by Schwarz at 2200–2300 cm^{-1} [Schwarz, H. A. *J. Chem. Phys.* **1977**, 67, 5525–5534] and vibrational predissociation spectrum by Lee et al. $\sim 2300 \text{ cm}^{-1}$ [Okumura, M.; Yeh, L. I.; Myers, J. D.; Lee, Y. T. *J. Chem. Phys.* **1990**, 94, 3416–3427].

1. Introduction

The study of ions in water raises many interesting questions about charge transfer mechanisms and dynamics in liquid water.^{1–4} The nature and transport mechanism of the proton in aqueous solutions and its spectroscopic signatures have been the subject of extensive discussions for many years.^{5–7} Protons (H^+) and hydroxide ions (OH^-) exhibit anomalously high mobility in aqueous media compared to other ions, such as sodium (Na^+) and chloride (Cl^-) ions,⁸ indicating that transport occurs via mechanism other than normal ionic diffusion. This phenomenon immediately introduces the crucial role of H_3O^+ and H_5O_2^+ that are ion cores of so-called Eigen⁹ and Zundel¹⁰ forms of the cations, respectively. Fluctuations between these species are thought to mediate the Grotthuss mechanism¹¹ for proton transport.

A powerful way to test the validity of various theoretical models is through the use of the cluster ions, e.g., $\text{H}^+(\text{H}_2\text{O})_n$

and $\text{OH}^-(\text{H}_2\text{O})_n$ which can be prepared and isolated in the laboratory. It is of significant interest to study clusters of larger size, because the structure and behavior of small hydrated proton clusters are quite different from those of larger size. The most obvious difference is that smaller clusters do not favor the ring structure which gives the maximum number of hydrogen bonds.¹² A recent study shows that proton transfer along hydrogen-bonded water chains can be facilitated by H_7O_3^+ .¹³

The motivation for this study is to explain the proton transfer mechanics in H_7O_3^+ for which theoretical and experimental studies are limited and global potential energy surface is not available. DFT direct molecular dynamics simulations of H_7O_3^+ in the gas phase were first performed using the B3LYP functional for a short simulation time (2 ps)¹⁴ and the spectral peaks assigned using NMA. Simulated IR spectra reproduced the observed IR pattern,¹⁵ and the broad region between 2200–2300 cm^{-1} was assigned to a stretch of bridging protons. The H_7O_3^+ spectrum in the OH stretch region was studied experimentally by Lee et al.¹⁶

* Corresponding author phone: +1-770-423-6281; fax: +1-770-423-6744; e-mail: mkaledin@kennesaw.edu.

They observed triplet signals at 3637, 3667, and 3722 cm^{-1} corresponding to a free OH symmetric H_2O stretch, H_3O^+ OH stretch, and free OH asymmetric H_2O stretch, respectively, and compared them to the spectra of $\text{H}_7\text{O}_3^+\cdot\text{H}_2$ at 3642, 3587, and 3726 cm^{-1} measured by vibrational predissociation spectroscopy.¹⁷ When authors searched for spectra of H_7O_3^+ down to 2200 cm^{-1} , a broad absorption was found below 2500 cm^{-1} , but due to low laser energy, their results were inconclusive. In this experimental work,¹⁷ the hydrogen bonded OH stretch in H_5O_4^+ at 2670 cm^{-1} was observed that largely agreed with Schwarz's results.¹⁵ Isotope dependence of proton exchange and reactions of protonated water clusters $\text{H}^+(\text{H}_2\text{O})_n$ ($n = 1-4$) with D_2O and $\text{D}^+(\text{D}_2\text{O})_n$ ($n = 1-4$) with H_2O were studied using guided ion beam mass spectroscopy.¹⁸ At low collision energies, H-D exchange product ions were observed as well as solvent exchange reaction products.¹⁸

Recently, Duncan et al.¹⁹ reported photodissociation infrared spectra of water clusters $\text{H}^+(\text{H}_2\text{O})_n$ ($n = 2-5$) with and without Ar tagging. Their experimental studies were complemented by computational work at the MP2/aug-cc-pVTZ level of theory. The H_7O_3^+ without Ar yields broad-defined resonances due to the fact that the photodissociation signal was weak. The spectrum measured with Ar contains three main bands at 3577, 3638, and 3722 cm^{-1} ; those were compared to the triplet observed by Lee et al.¹⁶ They also found a small, but reproducible, feature at 3098 cm^{-1} and assigned it to the overtone of the water scissors motion predicted at 1599/1623 cm^{-1} .

Spectral signatures of hydrated proton vibrations in water clusters $\text{H}^+(\text{H}_2\text{O})_n$ ($n = 2-11$) were characterized by vibrational predissociation spectroscopy²⁰ and assigned by anharmonic VSCF calculations.²¹ The vibrational spectrum of the Eigen cation $\text{H}^+(\text{H}_2\text{O})_4$ shows a strong band at 2665 cm^{-1} that correspond to symmetric and asymmetric H_3O^+ stretches. After removal of one water from $\text{H}^+(\text{H}_2\text{O})_4$, the spectrum of $\text{H}^+(\text{H}_2\text{O})_3$ shows a dramatic splitting of the $\text{H}^+(\text{H}_2\text{O})_4$ strong feature at 1880 and 3580 cm^{-1} . Therefore, anharmonic corrections are required to describe the large redshifts in $\text{H}^+(\text{H}_2\text{O})_3$ stretching transitions. The peaks at 1880 and 3580 cm^{-1} were assigned to asymmetric H_3O^+ stretch and H_3O^+ free OH stretch vibrations using anharmonic VSCF calculations.

Experimental spectra are often analyzed with the aid of theoretical calculations. Ab initio molecular dynamics simulations contribute to the gaining of insight into the process of solvation of OH^- and H^+ ions. From these simulations, structural as well as dynamical properties of these systems can be investigated. We present IR spectra obtained from the direct MD approach. The accuracy and feasibility of this approach were tested and verified on the smaller well studied molecular system, H_3O_2^- .²² Recently, a classical method of assignment of the spectral features using driven molecular dynamics (DMD) method²³ has been proposed. This method was originally developed to calculate the normal mode frequencies and normal mode vectors of large molecules.^{24,25} We used the DMD method to analyze unassigned, anharmonic spectral features in the H_5O_2^+ infrared spectrum.²⁶ Simulated IR spectra reproduced the patterns in the experi-

mental spectra and the assignment of IR bands. In this work, we use DMD to identify the shared proton vibrations in the IR spectrum of H_7O_3^+ beyond the harmonic normal-mode analysis.

2. Computational Details

A. Potential Energy Surface. We have studied the structural isomers, energetics, and IR spectra of H_7O_3^+ protonated water cluster. All electronic structure calculations were performed by using the Gaussian 03 program package.²⁷ The geometries of H_7O_3^+ stationary points were fully optimized using the density functional theory (DFT) with B3LYP²⁸⁻³⁰ functional and 6-31+G** basis set. The second order Møller–Plesset (MP2) perturbation theory³¹⁻³³ optimizations with the cc-pVTZ and aug-cc-pVTZ basis sets were performed as well, in order to validate predictions of DFT-B3LYP. The CCSD(T)/cc-pVTZ energies were obtained using the single-point energy calculations on the MP2/cc-pVTZ geometries. The vibrational frequencies for H_7O_3^+ and its D-substituted isotopologues were obtained using the standard NMA.³⁴ The dissociation energies of H_7O_3^+ to $\text{H}_2\text{O} + \text{H}_5\text{O}_2^+$ and H_5O_2^+ to $\text{H}_2\text{O} + \text{H}_3\text{O}^+$ were estimated at various levels of theory.

B. Direct Molecular Dynamics. IR spectra of H_7O_3^+ and D-substituted isotopologues were obtained by propagating trajectories on the fly at the B3LYP/6-31+G** level of theory. The interaction potential, forces, and dipole were computed at every time step. The simulations were carried out on our Linux computer cluster using a shell script that interfaces the Gaussian 03 program and our own suite of MD codes.

Two different kinds of direct MD simulations were performed to study the system. The starting point for all trajectories was the equilibrium structure with randomly sampled velocities from the Boltzmann distribution. Initially the system was equilibrated for the first 500 steps (250 fs). The first set of simulations was performed under constant temperature (NVT) conditions, and results from these simulations were used to analyze the structural features of the H_7O_3^+ water cluster. Ten trajectories were propagated at a constant temperature via Berendsen's thermostat.³⁵ The constant temperature was maintained with a 10 fs time response parameter.³⁵ A second set of simulations, also from 10 trajectories, was performed at constant energy (NVE) conditions. The results from these simulations were used to analyze the dynamical properties calculated using time correlation function. Spectra were collected for $J = 0$ using the expression for the intensity I

$$I(\omega) = \frac{\text{Re}}{\pi} \int_0^\infty dt e^{i\omega t} \langle \vec{\mu}(0) \cdot \vec{\mu}(t) \rangle_T \quad (1)$$

where ω is the frequency, $\langle \vec{\mu}(0) \cdot \vec{\mu}(t) \rangle_T$ is the dipole–dipole correlation function at temperature T .

The initial coordinates and momenta for the NVE ensembles were sampled from the previously run equilibrated NVT trajectories, and then the spectra were calculated by the Fourier transform of the dipole–dipole correlation function multiplied by a quantum mechanical frequency-

dependent factor³⁶ equal to $\omega/[1 - \exp(-\omega/kT)]$. The correlation function in eq 1 was obtained as a time average along the trajectory³⁷ to yield better converged spectra. We checked conservation of the total angular momentum and the energy to ensure the accuracy of the propagator.

In order to facilitate the spectral assignment of the peaks, we calculate position–position spectra for certain atomic groups and dipole spectra from the dipole–dipole correlation function decomposed into parallel and perpendicular components $\langle \mu_y(0)\mu_y(t) + \mu_z(0)\mu_z(t) \rangle_T$ and $\langle \mu_x(0)\mu_x(t) \rangle_T$, respectively. Details of these two methods can be found in our recent paper on H_3O_2^- .²²

C. Driven Molecular Dynamics. The most dominant spectral features were assigned using the driven molecular dynamics (DMD) method.²⁴ The DMD method was originally used to calculate the normal mode frequencies and normal mode vectors of large molecules for which the standard Hessian-based methods are not feasible due to the high memory and disk requirements.²⁵ The important advantage of DMD over the Hessian-based normal-mode analysis is the ability to study anharmonic motion and mode coupling.

The DMD method uses an external, sinusoidal driving source to identify resonant absorptions. To identify a resonant vibrational mode in the spectrum, the vibrational motion associated with that mode must produce a change in the dipole moment of the molecule. At resonant frequencies, the molecular motions induced by a weak driving force (small perturbation) correspond to infrared active frequencies, while harder driving (stronger perturbation) induces anharmonic motion.

In DMD simulations of vibrational IR spectra, the Hamiltonian of a molecular system, H

$$H(\mathbf{p}, \mathbf{q}, t; \omega) = H_0(\mathbf{p}, \mathbf{q}) + U(\mathbf{q}, t; \omega) \quad (2)$$

consists of the free molecular Hamiltonian, $H_0 = V(\mathbf{q}) + \mathbf{p}^2/2m$, where V is the molecular potential and a dipole-driving term $U(\mathbf{q}, t; \omega)$

$$U(\mathbf{q}, t; \omega) = \vec{\epsilon}_0 \cos(\omega t) \vec{\mu}(\mathbf{q}) \quad (3)$$

\mathbf{q} and \mathbf{p} are the $3N$ atomic Cartesian coordinates and momenta, respectively, ω is frequency, t is time, $\vec{\epsilon}_0$ determines the direction and strength of the electric field, and $\vec{\mu}(\mathbf{q})$ is the electric dipole of the molecule. Hamilton's equations of motion for Cartesian coordinate α of atom i are

$$\begin{aligned} \dot{q}_{\alpha,i} &= \frac{\partial H}{\partial p_{\alpha,i}} = \frac{p_{\alpha,i}}{m_i}, \\ \dot{p}_{\alpha,i} &= -\frac{\partial H}{\partial q_{\alpha,i}} = -\frac{\partial V}{\partial q_{\alpha,i}} - \epsilon_{0,\alpha} \cos(\omega t) \frac{\partial \mu_{\alpha}}{\partial q_{\alpha,i}}; \\ i &= 1, \dots, N, \alpha = x, y, z \end{aligned} \quad (4)$$

The dipole moment and dipole derivatives of the system are defined as follows:

$$\begin{aligned} \vec{\mu} &= \sum_{i=1}^N \vec{q}_i Q_i \\ \frac{\partial \vec{\mu}}{\partial \vec{q}_i} &= \delta_{\alpha\beta} Q_i; \quad \alpha, \beta = x, y, z \end{aligned} \quad (5)$$

Dipole derivative is not generally computed in single energy and gradient calculations. We approximated the dipole derivative using atomic charges from Mulliken population analysis³⁸ assuming that atomic charges vary slowly along the trajectory.

To identify resonant frequencies, the average internal energy of the molecule is obtained after a finite time of driving, which is given by

$$\langle E \rangle = \frac{1}{t - t_0} \int_{t_0}^t H(\tau) d\tau \quad (6)$$

where t_0 is some initially chosen time elapsed after the start of propagation. At nonresonant frequencies, the absorbed energy is small and oscillatory with time, while on resonance, whether fundamental or nonfundamental frequency, it increases rapidly with time. DMD simulations were carried out for several frequencies of interest.

At a resonant frequency a DMD trajectory shows oscillations of atoms around their equilibrium positions with the amplitudes proportional to the absorbed energy. A procedure of assignment of particular frequency consists of analysis of the atomic motion from DMD simulations in terms of the standard normal modes.²⁶ We evaluate normalized mass-scaled atomic displacements from DMD simulations after a significant amount of energy is absorbed by the molecule, after time t_0 (see eq 6)

$$\Delta x_i(t) = \frac{m_i^{1/2}(q_{ti} - q_{ei})}{[\sum_{i=1}^{3N} m_i(q_{ti} - q_{ei})^2]^{1/2}} \quad (7)$$

Then, a comparison of two modes is done by calculation the inner product of the DMD displacement $\Delta x(t)$ and standard normal mode

$$O_j(t) = \Delta x(t) \cdot u_j = \sum_{i=1}^{3N} \Delta x_i(t) u_{ij} \quad (8)$$

where u_j is the j th normal mode vector. The overlap is expected to be 1.0 if the two sets of vectors are identical and 0.0 if they are uncorrelated. This procedure was tested extensively on H_5O_2^+ ²⁶ and is capable of identifying combination bands which are absent in the NMA model.

3. Potential Energy Surface

A. Stationary Points. The orientation of H_7O_3^+ in the coordinate system and the atom labeling are shown in Figure 1. The global minimum of H_7O_3^+ is of C_s symmetry. The structural parameters (Table 1) obtained at the B3LYP/6-31+G**, MP2/cc-pVTZ, and MP2/aug-cc-pVTZ levels of theory are very similar. The bond lengths are within 0.01 Å except the proton stretch coordinate, $R(\text{O}_2-\text{H}_5)$. The proton transfer coordinate is particularly sensitive to the basis set and the method. According to the previous B3LYP calculations¹⁴ using the relatively small basis set DZP basis set for hydrogen and TZP for oxygen atoms, this stretching coordinate is 1.415 Å, while at DFT-B3LYP/6-31+G** and

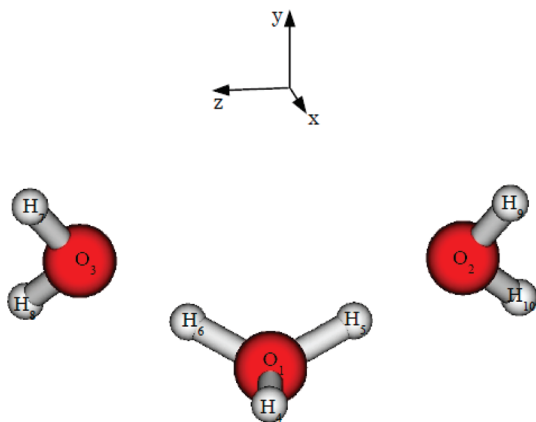


Figure 1. MP2 minimum structure (C_s) and the atom labeling.

MP2/aug-cc-pVTZ levels of theory $R(\text{O}_2-\text{H}_5)$ is 1.435 Å, 1.453 Å, respectively.

Vibrational frequencies for H_7O_3^+ are listed in Table 2. The vibrational frequencies and mode assignment are very similar for both B3LYP and MP2 methods, except of a few low frequency modes. The important qualitative features in the spectrum are the bridging hydrogen bending modes (agree within 40 cm^{-1}), bridging hydrogen stretching mode (within 80 cm^{-1}), and OH stretching modes (within 20 cm^{-1}). In order to assign the spectral peaks in our classical MD spectra, we report spectra for various deuterium isotopologues, D_7O_3^+ , DH_6O_3^+ , and $\text{D}_3\text{H}_4\text{O}_3^+$.

There are several stationary points on the potential energy surface of the protonated water cluster, H_7O_3^+ (Figure 2). The low-energy transition structure (TS1) of C_{2v} symmetry was found in the previous theoretical work.¹⁴ This planar transition state connects two pyramidal H_3O^+ configurations. The reaction mode represents the umbrella motion of the H_3O^+ ion. The energy differences between the global minimum of C_s symmetry

Table 1. H_7O_3^+ Minimum Structure Using the DFT-B3LYP and MP2 Methods

internal coordinates ^a	B3LYP/6-31+G**	MP2/cc-pVTZ	MP2/aug-cc-pVTZ
$R_1(\text{O}_1-\text{H}_4)$ Å	0.969	0.965	0.967
$R_2(\text{O}_1-\text{H}_5)$ Å	1.047	1.038	1.038
$R_3(\text{O}_2-\text{H}_5)$ Å	1.435	1.443	1.453
$R_4(\text{O}_2-\text{H}_9)$ Å	0.967	0.962	0.964
$R_5(\text{O}_2-\text{H}_{10})$ Å	0.968	0.963	0.965
$\alpha_1(\text{H}_4-\text{O}_1-\text{H}_5)$ deg	114.1	112.1	112.1
$\alpha_2(\text{H}_5-\text{O}_1-\text{H}_6)$ deg	118.4	114.6	114.6
$\alpha_3(\text{H}_5-\text{O}_2-\text{H}_9)$ deg	127.3	125.4	125.5
$\alpha_4(\text{H}_5-\text{O}_2-\text{H}_{10})$ deg	123.4	121.0	121.3
$\alpha_5(\text{H}_9-\text{O}_2-\text{H}_{10})$ deg	108.8	106.8	106.9
$\alpha_6(\text{O}_1-\text{H}_5-\text{O}_2)$ deg	176.3	174.5	174.3
$\delta_1(\text{H}_4-\text{O}_1-\text{H}_5-\text{O}_2)$ deg	114.2	156.7	154.8
$\delta_2(\text{H}_5-\text{O}_1-\text{H}_6-\text{O}_3)$ deg	107.3	73.9	76.0
$\delta_3(\text{H}_7-\text{O}_3-\text{H}_6-\text{O}_1)$ deg	179.4	160.9	161.8
$\delta_4(\text{H}_8-\text{O}_3-\text{H}_6-\text{O}_1)$ deg	7.9	52.0	49.8

^a The labeling of the atoms is shown on the Figure 1.

Table 2. H_7O_3^+ and D_7O_3^+ Vibrational Frequencies in cm^{-1}

tentative assignment	B3LYP/6-31+G**		MP2/aug-cc-pVTZ	
	H_7O_3^+	D_7O_3^+	H_7O_3^+	D_7O_3^+
MP2, sym OO stretch; B3LYP, H_2O torsion	38 (A'')	28 (A'')	76 (A')	71 (A')
MP2, H_2O torsion; B3LYP, sym OO stretch	68 (A')	64 (A')	86 (A'')	61 (A'')
H_2O twisting, in phase	124 (A')	93 (A')	130 (A')	94 (A')
H_2O wagging, out of phase	142 (A'')	104 (A'')	242 (A'')	184 (A'')
H_2O wagging, in phase	182 (A')	133 (A')	256 (A')	192 (A')
H_3O^+ wagging	341 (A')	257 (A')	352 (A')	270 (A')
MP2, asym OO stretch; B3LYP, H_3O^+ wagging	386 (A')	332 (A')	369 (A'')	293 (A'')
MP2, H_2O rocking; B3LYP, asym OO stretch	388 (A'')	297 (A'')	405 (A'')	343 (A'')
H_2O rocking	409 (A'')	358 (A'')	403 (A')	354 (A')
H_2O rocking, H_3O^+ umbrella	437 (A')	350 (A')	486 (A')	375 (A')
H_3O^+ rocking	613 (A'')	436 (A'')	615 (A'')	438 (A'')
H_3O^+ twisting	1142 (A'')	821 (A'')	1077 (A'')	775 (A'')
H_3O^+ wagging	1234 (A')	896 (A')	1266 (A')	921 (A')
H_2O bend, out of phase	1591 (A'')	1149 (A'')	1605 (A'')	1166 (A'')
H_2O bend, in phase	1629 (A')	1189 (A')	1633 (A')	1201 (A')
BH sym bend	1660 (A')	1208 (A'')	1699 (A')	1226 (A')
BH asym bend	1668 (A'')	1218 (A')	1702 (A'')	1235 (A'')
BH asym stretch	2387 (A'')	1802 (A'')	2464 (A'')	1852 (A'')
BH sym stretch	2554 (A')	1839 (A')	2620 (A')	1888 (A')
H_2O OH sym stretch, out of phase	3798 (A'')	2736 (A'')	3788 (A'')	2730 (A'')
H_2O OH sym stretch, in phase	3799 (A')	2737 (A')	3789 (A')	2731 (A')
H_3O^+ OH stretch	3823 (A')	2786 (A')	3810 (A')	2775 (A')
H_2O OH asym stretch, out of phase	3903 (A'')	2865 (A'')	3896 (A'')	2857 (A'')
H_2O OH asym stretch, in phase	3904 (A')	2866 (A')	3896 (A')	2858 (A')

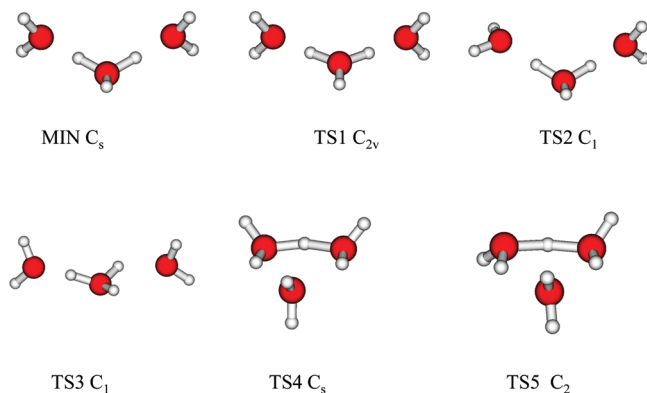


Figure 2. MP2 H_7O_3^+ stationary points.

Table 3. Energy Difference between the Stationary Points ($E_{C_s} - E_{C_{2v}}$) on the Potential Energy Surface of H_7O_3^+

method/basis set	$E_{C_s} - E_{C_{2v}}$ (kcal/mol)
B3LYP/6-31G**	0.61
B3LYP/6-31+G**	0.39
B3LYP/6-311G**	0.51
B3LYP/6-311+G**	0.43
MP2/cc-pVTZ	1.07
MP2/aug-cc-pVTZ	1.08
CCSD(T)/cc-pVTZ//MP2/cc-pVTZ	1.18
B3LYP/DZP(H)TZP(O) ¹⁴	0.69

and the transition state of C_{2v} symmetry obtained by various methods are listed in Table 3. The barrier height is sensitive to the choice of the basis set and correlation method. Our best estimate for the barrier height is 1.18 kcal/mol obtained from the CCSD(T)/cc-pVTZ single point energy calculations at the MP2/cc-pVTZ geometries. We found a transition state of C_1 symmetry (TS2) representing rotation of one of two waters. The rotational barrier is 0.65 kcal/mol at the B3LYP/6-31+G** level and 0.36 kcal/mol at the CCSD(T)/cc-pVTZ//MP2/cc-pVTZ computational level. Several high-energy transition states (with barrier heights about 5–7 kcal/mol) are shown in Figure 2 (TS3, TS4, TS5). The high-energy transition state (TS3 C_1) is assigned to the rotation of the hydronium ion. The barrier for rotation of H_3O^+ is much higher (6.8 kcal/mol), due to the presence of two hydrogen bonds between H_3O^+ and two H_2O compared to the rotational barrier of 0.36 kcal/mol for TS2 C_1 stationary point representing rotation of one of two waters within H_7O_3^+ . Pseudo-IRC calculations for the TS4 C_s and TS5 C_2 high-energy transition states show an interconversion of H_7O_3^+ from H_5O_2^+ to H_3O^+ ion cores.

B. Dissociation Energies. An important feature of the potential energy surface is the asymptotic region leading to the dissociation of H_7O_3^+ into the H_2O and H_5O_2^+ fragments. To estimate the influence of electron correlation on the dissociation energy, we carried out calculations of dissociation energy at various levels of theory (Table 4). For comparison, we report also $\text{H}_5\text{O}_2^+ \rightarrow \text{H}_2\text{O} + \text{H}_3\text{O}^+$ dissociation energy. With a comparison of our predictions of dissociation energy for H_5O_2^+ to the previous theoretical calculation³⁹ and experimental value,⁴⁰ our best estimate for the H_5O_2^+ dissociation energy is $D_e = 34.6$ kcal/mol at the MP2/aug-cc-pVTZ level of theory. Using the zero point energy (ZPE) of monomers and the ZPE of H_5O_2^+ calculated using harmonic approximation, we obtained $D_0 = 33.7$ kcal/

Table 4. H_5O_2^+ and H_7O_3^+ D_e Dissociation Energies and Zero Point Energy Corrected Values D_0 in kcal/mol

method/basis set	H_5O_2^+		H_7O_3^+	
	D_e	D_0	D_e	D_0
B3LYP/6-31G**	42.1	40.9	28.0	25.4
B3LYP/6-31+G**	37.6	36.6	25.0	22.5
B3LYP/6-311G**	40.8	39.7	27.8	25.3
B3LYP/6-311+G**	36.7	35.9	24.8	21.9
MP2/cc-pVTZ	36.9	35.9	25.2	22.4
MP2/aug-cc-pVTZ	34.6	33.7	23.6	20.7
CCSD(T)/cc-pVTZ//MP2/cc-pVTZ	36.1	35.2	24.9	22.1
CCSD(T)/aug-cc-pVTZ ³⁹	34.1			
exptl value of D_0 ⁴⁰		32.4		20.5

mol that agrees well with the experimental value reported by Dalleska et al., 32.4 kcal/mol.⁴⁰ Similarly, the best estimate for the H_7O_3^+ dissociation energy is $D_e = 23.6$ kcal/mol at the MP2/aug-cc-pVTZ level of theory. The ZPE corrected value $D_0 = 20.7$ kcal/mol is in a very good agreement with the experimental value of 20.5 kcal/mol.

4. Results from MD Simulations

A. Dipole Spectra. Dipole–dipole correlation functions were collected from 10 NVE trajectories propagated for 10 ps with a 0.5 fs time step at the energies roughly corresponding to each of the three temperatures, 100, 300, and 500 K. (See section 2B for details.) The error in the total energy was confined to less than 0.04% of the total energy for all trajectories.

It is usually sufficient to propagate a few such trajectories to achieve statistical convergence.²² The convergence of the spectrum at the B3LYP level was tested by comparing the shape of the dipole–dipole spectra from two sets of trajectories. The overlap of the spectra from 5 and 10 trajectories was 97%. The convergence of the position–position spectra was also satisfactory, within 96%.

Figure 3 presents the temperature dependence of the dipole spectrum of H_7O_3^+ calculated at the MD-B3LYP/6-31+G** level of theory from 500 to 4000 cm^{-1} , a spectral region

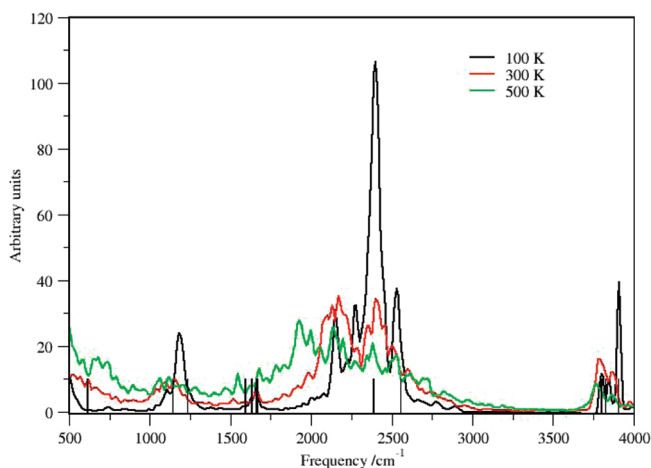


Figure 3. Temperature dependence of the MD B3LYP dipole–dipole spectra for H_7O_3^+ from 100 to 500 K. The IR spectra were obtained from 10 NVE trajectories propagated for 10 ps. The harmonic frequencies are shown as sticks in the spectrum.

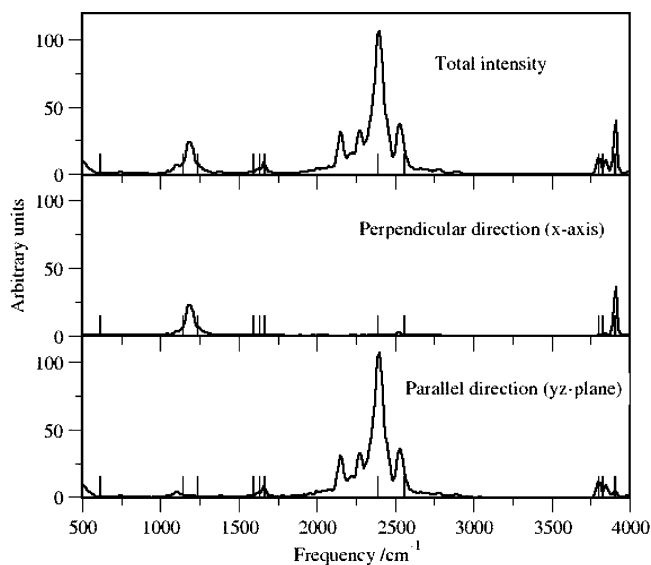


Figure 4. MD B3LYP spectrum for H_7O_3^+ at 100 K obtained from dipole–dipole correlation function $\langle \vec{\mu}(0) \cdot \vec{\mu}(t) \rangle_T$. The top panel shows the total intensity. The dipole–dipole correlation function was decomposed into perpendicular $\langle \mu_x(0) \cdot \mu_x(t) \rangle_T$ (along x-axis, middle panel) and parallel components $\langle \mu_y(0) \cdot \mu_y(t) + \mu_z(0) \cdot \mu_z(t) \rangle_T$ (along yz plane, bottom panel). The harmonic frequencies are shown as sticks in the spectrum.

relevant to the available experimental measurements. The harmonic frequencies are shown as sticks in the spectrum. At low temperature, 100 K, the MD simulations reproduce the harmonic spectrum. Significant deviation from the harmonic spectrum is seen between 2200 and 2800 cm^{-1} showing four peaks in the shared proton (bridging hydrogen, BH) stretch region at 100 K. At 500 K, this spectral feature significantly broadens.

In order to better understand the spectrum, the dipole spectrum at 100 K was decomposed into the parallel (yz plane) and perpendicular components (x axis) (Figure 4). All three oxygen atoms and two shared protons are positioned nearly in the yz plane. Therefore, the yz plane is coincident with the vibration of the shared proton between two oxygens (Figure 1). The most intense spectral peaks in the perpendicular dipole spectrum belong to the OH stretch vibrations. The broad spectral region between 2200 and 2800 cm^{-1} is due to the vibrations of those normal modes in the yz plane. The two peaks in this region at 2410 and 2540 cm^{-1} are assigned to the asymmetric and symmetric BH stretch vibration using NMA at the B3LYP/6-31+G** level of theory.

The identity of two weak spectral features at 2166 and 2275 cm^{-1} is scrutinized by means of the position–position spectra (Figure 5). This analysis reveals which atomic groups are involved in a particular vibration in a given spectral range. We analyzed three atomic groups, two oxygen atoms O2 and O3, two BH, H5 and H6 atoms, and four hydrogen atoms in two H_2O moieties, H7–H10. It is obvious that the most intense peaks around 390 cm^{-1} in the O2–O3 position–position spectrum and in the region 3800–3900 cm^{-1} in the H7–H10 position–position spectrum correspond to the OO stretch and OH stretch vibrations, respectively. There are several peaks present in the position–position spectrum for two shared

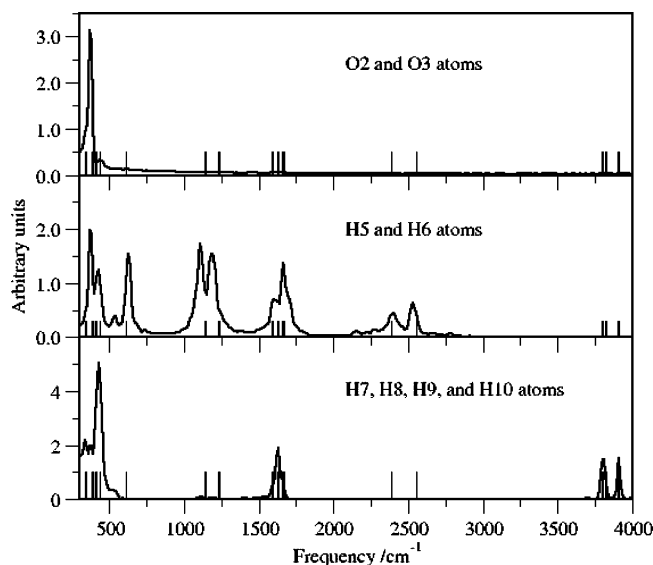


Figure 5. MD B3LYP position–position spectra decomposed to atomic groups at 100 K. The top panel shows the averaged spectrum for O2 and O3 oxygen atoms, the middle panel shows H5 and H6 bridging hydrogens, and the bottom panel shows H7, H8, H9, and H10 hydrogens. The labeling of the atoms is shown in Figure 1.

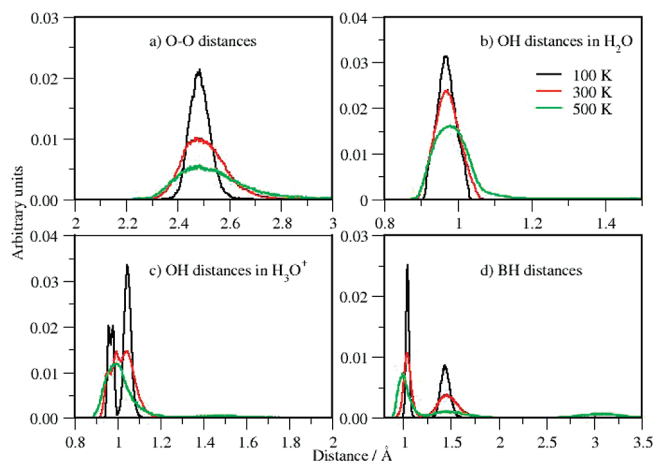


Figure 6. Temperature dependence of bond length distributions for H_7O_3^+ calculated from NVT MD-B3LYP trajectories at 100, 300, and 500 K. Each panel shows an average distribution over (a) O–O distances, (b) OH distances in H_2O , (c) OH distances in H_3O^+ , and (d) bridging hydrogen (BH) distances from oxygen in H_2O .

protons H5 and H6: those correlating with the normal mode frequencies (shown as sticks in the spectrum) umbrella vibration, rocking, twisting, and wagging H_3O^+ vibrations, BH bend vibrations, and BH stretch vibrations. See mode assignment in Table 2. This figure shows some activity between 2150 and 2300 cm^{-1} , which means that these vibrations most likely engage a shared proton.

B. Bond Length Distributions. We examined the bond length distributions for H_7O_3^+ calculated from the coordinates saved along the NVT MD-B3LYP/6-31+G** trajectories to determine favorable atomic configurations at temperatures between 100 and 500 K (Figure 6). At low temperature, 100 K, the distributions peaked at distances that are close to the equilibrium distances listed in Table 1, while

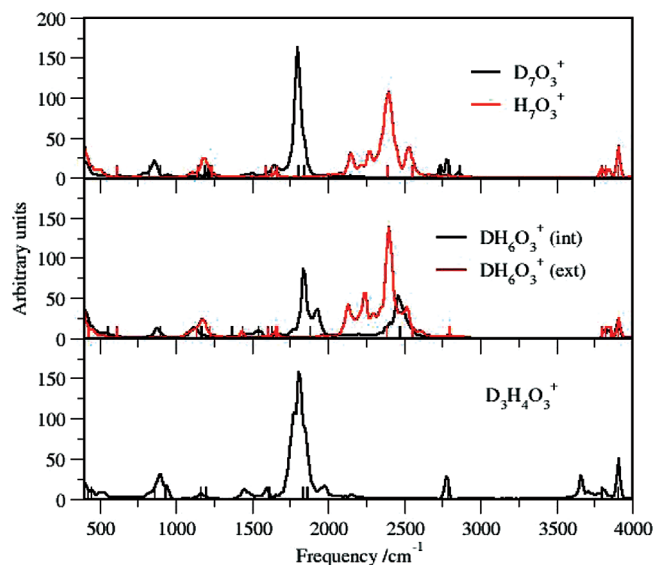


Figure 7. MD B3LYP dipole–dipole spectra at 100 K for H_7O_3^+ and its D-substituted isotopologues.

at higher temperatures, the bond length distributions broaden significantly and reveal various bonding topology changes. H_3O^+ in H_7O_3^+ is slightly asymmetric at equilibrium showing maxima at 0.97 and 1.05 Å (Figure 6c, 100 K). At 500 K all OH distances become equal to 1.0 Å corresponding to pure H_3O^+ (hydronium cation). The average distribution of bond lengths for two bridging hydrogens hopping between oxygens is showing two peaks around 1.05 and 1.44 Å at 100 K. With increasing temperature, the first peak shifts to the lower distance 1.0 Å, indicating a presence of hydronium cation, while the intensity of the second peak decreases significantly, indicating the presence of the H_5O_2^+ Zundel form of cation. Thus, we assume that proton hopping primarily occurs through an Eigen \rightarrow Zundel \rightarrow Eigen transition. During our simulations we did not observe formation of H_3O^+ and water dimer configurations as suggested in the previous work.¹⁴ However, at high temperature, 500 K, we observed frequent hydrogen exchange between H_3O^+ and H_2O as evidenced by a small peak around 3.25 Å (Figure 6d).

C. Effect of Isotopic Substitution. In the present study, we report vibrational spectra of D-substituted isotopologues D_7O_3^+ , DH_6O_3^+ , and $\text{D}_3\text{H}_4\text{O}_3^+$, calculated from MD-B3LYP trajectories at 100 K (Figure 7). In DH_6O_3^+ , multiple isomers are possible as deuterium can be located in the shared position between oxygen atoms (interior position designated as int in Figure 7) or in one of two H_2O (exterior position, ext). In the $\text{D}_3\text{H}_4\text{O}_3^+$ isomer, three deuterium atoms are located on hydronium ion core. OH (OD) stretch region of the spectra can be easily identified using the NMA. The D_7O_3^+ spectrum displays the dominant peak at 1800 cm^{-1} that can be assigned using the NMA to asymmetric and symmetric shared proton vibrations separated by 37 cm^{-1} (see Table 2). In the H_7O_3^+ spectrum, these frequencies are well resolved about 167 cm^{-1} apart. The unassigned weak spectral features in the H_7O_3^+ at 2166 and 2275 cm^{-1} are seen in the D_7O_3^+ spectrum as weak spectral features at 1500 and 1650 cm^{-1} .

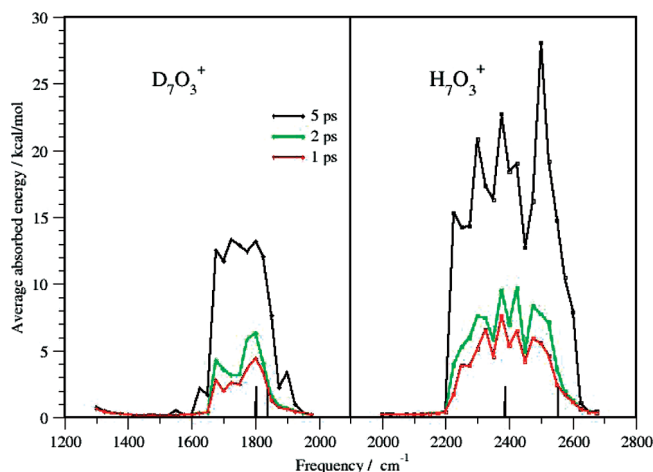


Figure 8. DMD B3LYP simulations: scanned spectrum with a 25 cm^{-1} step for H_7O_3^+ and D_7O_3^+ . For each frequency, a trajectory was propagated for 5 ps using $\bar{e}_0 = 50$ mV/bohr. The harmonic frequencies are shown as sticks in the spectrum.

DH_6O_3^+ spectra for interior (int) and exterior (ext) positions of deuterium are shown in the middle panel of Figure 7. Because zero-point energies for interior and exterior isomers are very similar, 17 432 and 17 424 cm^{-1} , respectively, we assume that experimental measurements would show the signature of both isomers. Interestingly, deuterium in the exterior position increases the spectral intensity of shared proton vibrations by about 20%. Two peaks in the DH_6O_3^+ (int) spectrum positioned at 1800 and 2470 cm^{-1} correspond to the shared D (H) vibrations, respectively. The nonfundamental spectral features present in the H_7O_3^+ spectrum are absent in the DH_6O_3^+ (int) spectrum. As will be discussed below, these bands arise probably from mixing of low frequency modes and BH stretch vibrations.

5. Results from DMD Simulations

DMD spectra were obtained by propagating trajectories for 5 ps, with the time step 0.5 fs for each frequency. Each trajectory was started at rest at the equilibrium structure. We tested the electric field, \bar{e}_0 , for a few strongly absorbing frequencies to select an appropriate field strength. The optimal field for most frequencies was found to be 50 mV/bohr, which corresponds to about 5% of the H_7O_3^+ dissociation energy and 0.5% of the first electronic excitation energy and leads to mild driving. We note that the first excitation energy for H_7O_3^+ is singlet A'' at 8.94 eV, calculated using TD-DFT with the B3LYP functional and 6-31+G** basis set.

Previous experimental studies¹⁵ concluded that bridging proton vibrations in H_7O_3^+ occur near 2200–2300 cm^{-1} . To capture IR activity in this region, we scanned the spectrum between 2000 and 2700 cm^{-1} and 1300 and 2000 cm^{-1} for H_7O_3^+ and D_7O_3^+ , respectively, with a 25 cm^{-1} frequency step. Figure 8 shows DMD spectra for H_7O_3^+ and D_7O_3^+ (averaged absorbed energy as a function of frequency). The longer the propagation time of the trajectory, the more energy is absorbed by the molecule. We analyzed DMD spectra obtained from trajectories propagated up to at 1, 2, and 5 ps

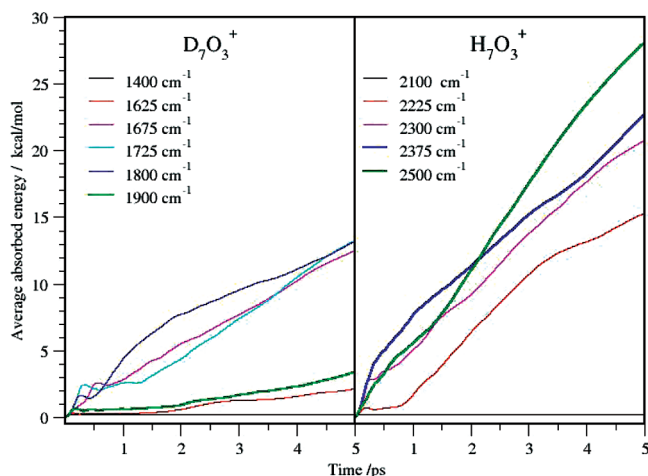


Figure 9. DMD B3LYP simulations: average absorbed energy as a function of time for H_7O_3^+ and D_7O_3^+ using $\bar{e}_0 = 50$ mV/bohr.

to identify anharmonic features. The short time simulations at or near fundamental frequencies reveal the harmonic vibrational spectra, while longer time driving at nonfundamental peaks causes the molecule to absorb enough energy to leave the harmonic region and give rise to absorptions due to mode coupling (see below).

The scanned DMD spectrum (Figure 8) for D_7O_3^+ shows peaks around $1700\text{--}1800\text{ cm}^{-1}$. The normal mode fundamental frequencies (displayed as sticks in the spectrum) for asymmetric and symmetric bridging hydrogen stretch for D_7O_3^+ are equal to 1802 and 1839 cm^{-1} , respectively. At longer driving simulation times, these peaks broaden, and weak features are seen at 1550 and 1900 cm^{-1} , similar to the IR spectrum shown in Figure 7. The maximum peaks of the average absorbed energies (eq 6) as a function of time are shown in Figure 9. At nonfundamental and absorbing frequencies (1400 cm^{-1} for D_7O_3^+ , 2100 cm^{-1} for H_7O_3^+), the absorbed energy is small and oscillatory with time, while at fundamental frequencies (maximum peaks at 1800 cm^{-1} for D_7O_3^+ , 2375 and 2500 cm^{-1} for H_7O_3^+) the absorbed energy increases rapidly with time. The absorption profiles for several nonfundamental frequencies (1625 , 1675 , 1725 , 1900 cm^{-1} for D_7O_3^+ and 2225 , 2300 cm^{-1} for H_7O_3^+) are more complex. The absorbed energy is small and oscillating until the system absorbs enough energy and escapes the harmonic region of the potential energy surface. The moderate or rapid absorption is observed then. These frequencies are expected to be combination bands due to mode coupling.

Analysis of absorbing modes depends on the driving time as well as on the strength of the field. To study the effect of the strength of the electric field on the DMD simulations, we carried out a set of driven simulations using electric field strengths $\bar{e}_0 = 25$, 50 , and 75 mV/bohr for maximum peaks at 2225 and 2375 cm^{-1} in the DMD spectrum (Figure 8). Figure 10 shows the energy profiles as a function of driven time. The DMD peak at 2375 cm^{-1} represents a resonance with the normal mode at 2387 cm^{-1} , and it shows very little effect of the electric field strength on the absorbed energy profile, while driving at nonfundamental frequency 2225 cm^{-1} , the stronger the electric field, more energy is absorbed by the molecule at much shorter time. To resolve the weak

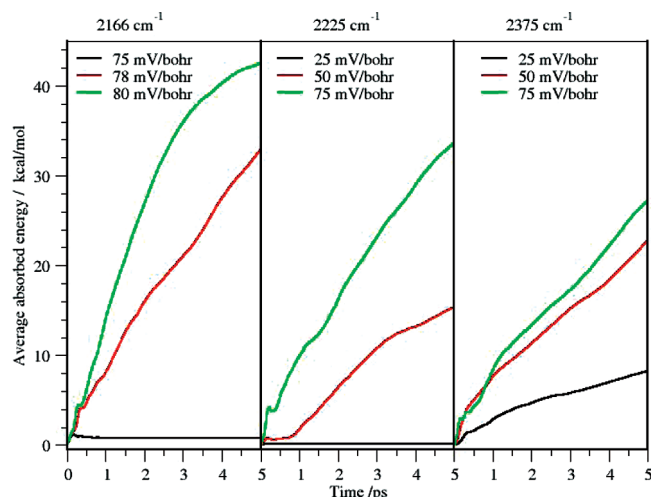


Figure 10. DMD B3LYP simulations: average absorbed energy in cm^{-1} as a function of time and an electric field strength for three driven frequencies $\omega = 2166$, 2225 , and 2375 cm^{-1} .

spectral feature at 2166 cm^{-1} found in the MD spectrum (Figure 4), we gradually increased the electric field, until the absorption of energy was identified. Dipole driving does not show much response for the electric field up to $\bar{e}_0 = 75$ mV/bohr, while the system started to absorb rapidly when the electric field $\bar{e}_0 = 78$ mV/bohr was applied.

To quantify similarities between the DMD displacements and normal mode vectors, the average overlaps (eq 8) and average weights²⁶ were calculated for each driven frequency. We analyzed the overlap matrix for two fundamental frequencies 2387 and 2554 cm^{-1} ($\bar{e}_0 = 50$ mV/bohr) corresponding to asymmetric and symmetric stretches of bridging hydrogen and for two nonfundamental frequencies 2166 ($\bar{e}_0 = 78$ mV/bohr) and 2225 cm^{-1} ($\bar{e}_0 = 50$ mV/bohr). At short simulation times, up to 100 fs, the average weights (diagonal elements of the overlap matrix) for fundamental frequencies 2387 and 2554 cm^{-1} are 0.435 and 0.204 , respectively. Off-diagonal elements of the overlap matrix are relatively small (less than 0.1). The average absorbed energy was only 0.7 and 0.5 kcal/mol, respectively. At longer driving times, 250 fs, the average absorbed energies have reached values 2.9 and 1.3 kcal/mol for frequencies 2387 and 2554 cm^{-1} , respectively, and the average weights for these two normal modes are only 0.299 and 0.247 . Also, we observed increasing torsion motion at all resonant frequencies. The analysis of the overlap matrix is meaningful shortly after the system hits the resonance and starts to absorb energy. We now analyze dipole driving for nonfundamental peaks at 2166 cm^{-1} using the electric field $\bar{e}_0 = 78$ mV/bohr, 2225 and 2300 cm^{-1} using $\bar{e}_0 = 50$ mV/bohr. Evident mixing among the modes is reflected in overlaps. The overlap matrix shows involvement of the H_2O in phase wagging, OO stretch, H_3O^+ rocking, and BH asymmetric stretch vibrations for nonfundamental frequencies. The overlaps with the normal mode vectors are relatively small, about 0.1 for H_2O in phase wagging, OO stretch, and H_3O^+ rocking modes, and 0.3 for BH asymmetric stretch vibrations.

To clarify the spectral assignment of the nonfundamental frequencies, we also monitored structural parameters along

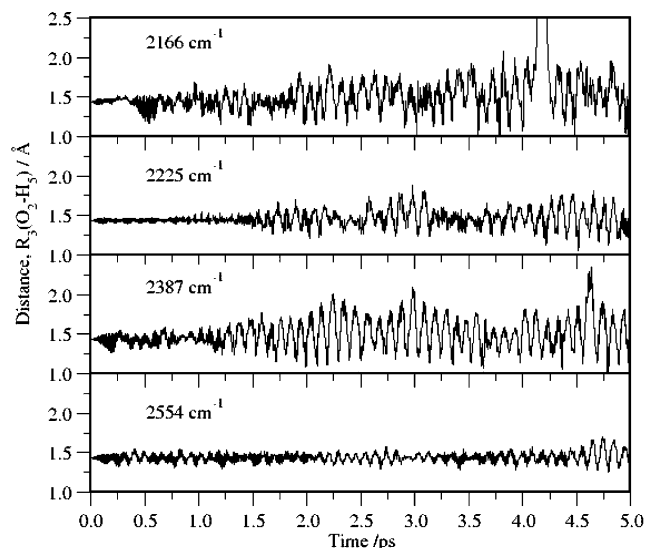


Figure 11. Results of DMD simulations: time dependence of the hydrogen bond $R_3(\text{O}_2\text{--H}_5)$. Atom numbering is shown in Figure 1. For driven frequencies $\omega = 2225, 2387$, and 2554 cm^{-1} , the electric field was $\bar{e}_0 = 50 \text{ mV/bohr}$, while for driven frequency $\omega = 2166 \text{ cm}^{-1}$, $\bar{e}_0 = 78 \text{ mV/bohr}$.

the DMD trajectory. Figure 11 shows time dependence of the hydrogen bond between O2 and H5 atoms. The atomic fluctuations increase with time until the system absorbs sufficient energy, and then O2–H5 distance fluctuates around the equilibrium value 1.435 \AA . In the case of 2387 cm^{-1} the atomic fluctuations are large comparing to the 2554 cm^{-1} frequency. Driving at 2166 cm^{-1} nonfundamental frequency shows a similar pattern of atomic fluctuations to ones at 2387 cm^{-1} , supporting our spectral assignment of 2166 cm^{-1} frequency to BH stretch. In the DMD trajectory propagated with $\omega = 2166 \text{ cm}^{-1}$, we observed proton exchange in the system at 4.2 ps . In this simulation, the maximum absorbed energy reaches 28 kcal/mol . In the case of nonfundamental frequency 2225 cm^{-1} , the bridging hydrogen fluctuations are relatively small up to 1.5 ps . The maximum absorbed energy at this point was about 2.8 kcal/mol . This is probably a threshold energy the system must absorb in order to activate this vibration. Visualization of the DMD trajectory demonstrates that the atomic motion acquires significant torsion character almost at all resonant frequencies. We plot the angle between the two planes H5–O1–H4 and H9–O2–O10 (Figure 12) to describe the torsion motion. Fluctuations of bridging hydrogen and torsion angle show similar patterns along the DMD trajectory that imply possible mixing between these modes.

6. Conclusions

(a) In this work, we present new results on analysis of the potential energy surface. Several stationary points on the PES of H_7O_3^+ were identified. They are the high energy transition states with barrier heights about $5\text{--}7 \text{ kcal/mol}$ and the low energy transition structures that represent the umbrella motion of the H_3O^+ ion and rotation of one of two waters in H_7O_3^+ with 1.18 and 0.36 kcal/mol barrier heights at CCSD(T)/cc-pVTZ //MP2/cc-pVTZ level of theory, respectively.

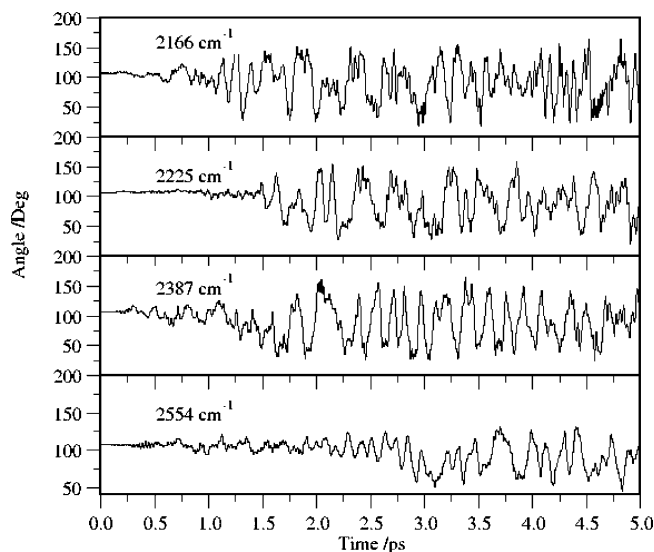


Figure 12. Time dependence of the torsion angle between two planes H5–O1–H4 and H9–O2–H10. For driven frequencies $\omega = 2225, 2387$, and 2554 cm^{-1} , the electric field was $\bar{e}_0 = 50 \text{ mV/bohr}$, while for driven frequency $\omega = 2166 \text{ cm}^{-1}$, $\bar{e}_0 = 78 \text{ mV/bohr}$.

The dissociation energies of $\text{H}_3\text{O}^+ \cdot (\text{H}_2\text{O})_n$ for loss of one H_2O are 33.7 and 20.7 kcal/mol for $n = 1$ and $n = 2$ at the MP2/ug-cc-pVTZ level compared to 32.4 and 20.5 kcal/mol experimental values.⁴⁰

(b) The dipole spectra were obtained for $100, 300$, and 500 K at the B3LYP/6-31+G** level of theory and compared to previous theoretical calculations and experimental measurements. In this work, our focal point was analysis of shared proton vibrations. The spectra are decomposed to the parallel and perpendicular components to identify symmetry related vibrations. We also evaluated position–position spectra to analyze vibrations in terms of atomic groups. On the basis of NMA, the spectral peaks at 2410 and 2540 cm^{-1} were assigned to the asymmetric and symmetric bridging hydrogen stretch vibrations similar to the assignment in the previous theoretical work.¹⁴ However, the previous theoretical work did not analyze the weak spectral feature around 2000 cm^{-1} . Using polarized dipole–dipole spectra and position–position spectra, we assigned the weak spectral features at 2166 and 2275 cm^{-1} to bridging hydrogen vibrations.

The effect of isotopic substitution was analyzed. We reported vibrational spectra of several D-substituted isotopologues D_7O_3^+ , DH_6O_3^+ , and $\text{D}_3\text{H}_4\text{O}_2^+$. Our simulations can guide future experimental measurements similar to experimental H/D isotopic studies done for $\text{H}_5\text{O}_2^+ \cdot \text{Ar}$.^{41,42}

(c) Bond length distributions for H_7O_3^+ for temperatures $100, 300$, and 500 K indicate the presence of both Eigen-based and Zundel ion cores in the MD simulations of H_7O_3^+ . The simulations do not reveal formation of H_3O^+ and water dimer configurations as suggested in the previous work;¹⁴ however, at high temperature 500 K , we observed frequent hydrogen exchange between H_3O^+ and H_2O .

(d) The emphasis of this paper was the development and implementation of the driven molecular dynamics method to assign the spectral features. This is a first attempt to run

direct DMD simulations. The challenging part is to select the electric field strength and to determine the simulation time to obtain meaningful results. DMD simulations with weak electric field and short simulation times reproduce the harmonic features, while using higher intensity electric field and longer simulation times reveals anharmonic features. The scanned DMD spectrum can be correlated directly to the spectrum from the classical MD simulations. The average absorbed total energy was monitored as a function of driven frequency. DMD simulations confirm the assignment of the dominant peaks at 2410 and 2540 cm^{-1} to asymmetric and symmetric bridging hydrogen vibrations. The nonfundamental frequencies at 2166, 2225, and 2300 cm^{-1} were assigned to a combination band of BH asymmetric stretch, H_2O in phase wagging, OO stretch, and H_3O^+ rocking vibrations by DMD simulations. We evaluated overlap matrix to quantify the involvement of a certain vibration in the spectral feature. Analysis of the molecular motion along the DMD trajectories also guided the assignment of the spectral features. Visualization of the DMD trajectory demonstrates that the atomic motion acquires significant torsion character almost at all resonant frequencies.

(e) Our observation of BH stretch vibrations as low as 2166 cm^{-1} is in good agreement with the assignment of the low-resolution spectrum obtained by Schwarz at 2200–2300 cm^{-1} and the assignment of the $\text{H}_7\text{O}_3^+ \cdot \text{H}_2$ spectrum by Lee at $\sim 2300 \text{ cm}^{-1}$. However, we did not observe asymmetric and symmetric bridging hydrogen vibrations at 1880 and 3580 cm^{-1} as reported by recent Ar-tagged predissociation spectra.²⁰ The authors concluded that anharmonic corrections are required to qualitatively recover the large observed red shifts to describe $\text{H}^+(\text{H}_2\text{O})_3$ stretching transitions.

Quantum dynamics study would help to resolve uncertainties in the experimental observations of the shared proton vibrations; however, this would be computationally challenging. Also, the perturbations of the H_7O_3^+ spectrum by attached argon atom have to be evaluated. Previous calculations indicate a strong effect of an Ar messenger atom on H_5O_2^+ spectra.⁴³ The $\text{O}-\text{H}^+-\text{O}$ asymmetric stretch mode is significantly blue-shifted in $\text{H}_5\text{O}_2^+ \cdot \text{Ar}$. We believe that the present study provides new insight into the shared proton vibrations of H_7O_3^+ system and its D-substituted isotopologues and describes the application of the DMD method to assign spectral features.

Acknowledgment. The authors thank the Research Corporation (Cottrell College Science Award 7725) for support of this work.

References

- (1) Marx, D.; Tuckerman, M. E.; Hutter, J.; Parrinello, M. *Nature* **1999**, *397*, 601–604.
- (2) Marx, D.; Tuckerman, M. E.; Parrinello, M. *J. Phys.: Condens. Matter* **2000**, *12*, A153–A159.
- (3) Paesani, F.; Zhang, W.; Case, D. A.; Cheatham, T. E., III; Voth, G. A. *J. Chem. Phys.* **2006**, *125*, 184507.
- (4) Iyengar, S. S.; Petersen, M. K.; Day, T. J. F.; Burnham, C. J.; Teige, V. E.; Voth, G. A. *J. Chem. Phys.* **2005**, *123*, 084309.
- (5) Zundel, G. In *The Hydrogen Bond: Recent Developments in Theory and Experiment*; Schuster, P., Zundel, G., Sandorfy, C., Eds.; North Holland: Amsterdam, 1976; Vol. 2, p 683.
- (6) Giguere, P. A.; Turell, S. *Can. J. Chem.* **1976**, *54*, 3477–3482.
- (7) Librovich, N. B.; Sakun, V. P.; Sokolov, N. D. *Chem. Phys.* **1979**, *39*, 351–366.
- (8) Atkins, P. W.; de Paula, J. *Physical Chemistry*, 8th ed.; Freeman: New York, 2002; p 763.
- (9) Eigen, M.; Wicke, E. *J. Phys. Chem.* **1954**, *58*, 702–714.
- (10) Zundel, G.; Metzger, H. Z. *Phys. Chem. (Munich)* **1968**, *58*, 225–241.
- (11) Agmon, N. *Chem. Phys. Lett.* **1995**, *244*, 456–462.
- (12) Wei, D.; Salahub, D. R. *J. Chem. Phys.* **1994**, *101*, 7633–7642. Wei, D.; Salahub, D. R. *J. Chem. Phys.* **1997**, *106*, 6086–6094.
- (13) Yan, S.; Zhang, L.; Cukier, R. I.; Bu, Y. *Chem. Phys. Phys. Chem.* **2007**, *8*, 944–954.
- (14) Termath, V.; Sauer, J. *Mol. Phys.* **1997**, *91*, 963–975.
- (15) Schwarz, H. A. *J. Chem. Phys.* **1977**, *67*, 5525–5534.
- (16) Yeh, L. I.; Okumura, M.; Myers, J. D.; Price, J. M.; Lee, Y. T. *J. Chem. Phys.* **1989**, *91*, 7319–7390.
- (17) Okumura, M.; Yeh, L. I.; Myers, J. D.; Lee, Y. T. *J. Chem. Phys.* **1986**, *85*, 2328–2329. Okumura, M.; Yeh, L. I.; Myers, J. D.; Lee, Y. T. *J. Chem. Phys.* **1990**, *94*, 3416–3427.
- (18) Honma, K.; Armentrout, P. B. *J. Chem. Phys.* **2004**, *121*, 8307–8320.
- (19) Doublerly, G. E.; Walters, R. S.; Cui, J.; Jordan, K. D.; Duncan, M. A. *J. Phys. Chem. A* **2010**, *114*, 4570–4579.
- (20) Headrick, J. M.; Diken, E. G.; Walters, R. S.; Hammer, N. I.; Christie, R. A.; Cui, J.; Myshakin, E. M.; Duncan, M. A.; Johnson, M. A.; Jordan, K. D. *Science* **2005**, *308*, 1765–1769.
- (21) Chaban, G. M.; Jung, J. O.; Gerber, R. B. *J. Chem. Phys.* **1999**, *111*, 1823–1829.
- (22) Kaledin, M.; Moffitt, J. M.; Clark, C. R.; Rizvi, F. J. *J. Chem. Theory Comput.* **2009**, *9*, 1328–1336.
- (23) Bowman, J. M.; Zhang, X.; Brown, A. J. *J. Chem. Phys.* **2003**, *119*, 646–650.
- (24) Kaledin, M.; Brown, A.; Kaledin, A. L.; Bowman, J. M. *J. Chem. Phys.* **2004**, *121*, 5646–5653.
- (25) Kaledin, M.; Kaledin, A. L.; Brown, A.; Bowman, J. M. In *Normal Mode Analysis: Theory and Applications to Biological and Chemical Systems*; Cui, Q., Bahar, I., Eds.; CRC Press: Boca Raton, FL, 2006.
- (26) Kaledin, M.; Kaledin, A. L.; Bowman, J. M. *J. Phys. Chem. A* **2006**, *110*, 2933–2939.
- (27) Frisch, M. J.; Trucks, G. W.; Schlegel, H. B.; Scuseria, G. E.; Robb, M. A.; Cheeseman, J. R.; Montgomery, J. A., Jr.; Vreven, T.; Kudin, K. N.; Burant, J. C.; Millam, J. M.; Iyengar, S. S.; Tomasi, J.; Barone, V.; Mennucci, B.; Cossi, M.; Scalmani, G.; Rega, N.; Petersson, G. A.; Nakatsuji, H.; Hada, M.; Ehara, M.; Toyota, K.; Fukuda, R.; Hasegawa, J.; Ishida, M.; Nakajima, T.; Honda, Y.; Kitao, O.; Nakai, H.; Klene, M.; Li, X.; Knox, J. E.; Hratchian, H. P.; Cross, J. B.; Bakken, V.; Adamo, C.; Jaramillo, J.; Gomperts, R.; Stratmann, R. E.; Yazyev, O.; Austin, A. J.; Cammi, R.; Pomelli, C.; Ochterski, J. W.; Ayala, P. Y.; Morokuma, K.; Voth, G. A.; Salvador, P.; Dannenberg, J. J.; Zakrzewski, V. G.; Dapprich, S.; Daniels, A. D.; Strain, M. C.; Farkas, O.; Malick, D. K.;

- Rabuck, A. D.; Raghavachari, K.; Foresman, J. B.; Ortiz, J. V.; Cui, Q.; Baboul, A. G.; Clifford, S.; Cioslowski, J.; Stefanov, B. B.; Liu, G.; Liashenko, A.; Piskorz, P.; Komaromi, I.; Martin, R. L.; Fox, D. J.; Keith, T.; Al-Laham, M. A.; Peng, C. Y.; Nanayakkara, A.; Challacombe, M.; Gill, P. M. W.; Johnson, B.; Chen, W.; Wong, M. W.; Gonzalez, C.; and Pople, J. A. *Gaussian 03, Revision C.02*; Gaussian, Inc.: Wallingford, CT, 2004.
- (28) Lee, C.; Yang, W.; Parr, R. G. *Phys. Rev. B* **1988**, *37*, 785–789.
- (29) Becke, A. D. *J. Chem. Phys.* **1993**, *98*, 1372–1377.
- (30) Becke, A. D. *J. Chem. Phys.* **1993**, *98*, 5648–5652.
- (31) Head-Gordon, M.; Pople, J. A.; Frisch, M. J. *Chem. Phys. Lett.* **1988**, *153*, 503–506.
- (32) Saebo, M. J. S.; Almlöf, J. *Chem. Phys. Lett.* **1989**, *154*, 83–89.
- (33) Frisch, M. J.; Head-Gordon, M.; Pople, J. A. *Chem. Phys. Lett.* **1990**, *166*, 275–280.
- (34) Wilson, E. B.; Decius, J. C.; Cross, P. C. *Molecular Vibrations*; McGraw-Hill: New York, 1955.
- (35) Berendsen, H. J. C.; Postma, J. P. M.; Van Gunsteren, W. F.; Dinola, A.; Haak, J. R. *J. Chem. Phys.* **1984**, *81*, 3684–3690.
- (36) Berens, P. H.; Wilson, K. R. *J. Chem. Phys.* **1981**, *74*, 4872–4882.
- (37) Haile, J. M. *Molecular Dynamics Simulation: Elementary Methods*; Wiley & Sons: New York, 1992; p 277.
- (38) Mulliken, R. S. *J. Chem. Phys.* **1955**, *23*, 1833–1840.
- (39) Huang, X.; Braams, B. J.; Bowman, J. M. *J. Chem. Phys.* **2005**, *122*, 044308.
- (40) Dalleska, N. F.; Honma, K.; Armentrout, P. B. *J. Am. Chem. Soc.* **2003**, *115*, 12125–12131.
- (41) McCunn, L. R.; Roscioli, J. R.; Johnson, M. A.; McCoy, A. B. *J. Phys. Chem. B* **2008**, *112*, 321–327.
- (42) McCunn, L. R.; Roscioli, J. R.; Elliott, B. M.; Johnson, M. A.; McCoy, A. B. *J. Phys. Chem. A* **2008**, *112*, 6074–6078.
- (43) Park, M.; Shin, I.; Singh, N. J.; Kim, K. S. *J. Phys. Chem. A* **2007**, *111*, 10692–10702.

CT100122S